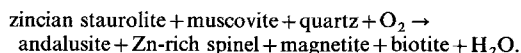


## Zincian staurolite in Glen Doll, Scotland

RENATE SCHUMACHER (née DÜRIG)

Mineralogisch-Petrologisches Institut, Universität Bonn, 5300 Bonn, W. Germany

**ABSTRACT.** Textures and relict mineralogy in the Dalradian gneisses from the southern contact aureole of the Glen Doll diorite trace the development of three stages of metamorphism through regional and contact metamorphic phases. Regional metamorphic stage I is characterized by the stability of sillimanite + muscovite; recognition of a subsequent regional metamorphic stage II of lower grade is based on textural criteria, the stability of kyanite and staurolite + quartz, and geothermometry/geobarometry. The breakdown of zincian staurolite occurred under the conditions of contact metamorphism (stage III). Textural evidence from the outer part of the contact aureole suggests that zincian staurolite broke down by the following oxidation reaction:



Various stages of completion of this reaction have been observed in different parts of a sample. Predominance of magnetite over Zn-rich spinel ( $\leq 14$  wt. % ZnO) as a breakdown product can be explained by the initial breakdown of Fe-staurolite component + muscovite + quartz + O<sub>2</sub> to form andalusite + biotite + magnetite. These product phases were joined by the Zn-rich spinel when sufficient Zn-staurolite component had concentrated in the unreacted staurolite. Rare local examples where Zn-rich spinel is dominant over magnetite may reflect lower O<sub>2</sub> fugacity and/or higher initial Zn contents of the staurolite.

**KEYWORDS:** staurolite, zinc, gneisses, Glen Doll, Scotland.

THE investigated area to the west of Glen Clova, Scotland, is one of the type localities of Barrovian metamorphism (Barrow, 1893, 1912*a, b*) (fig. 1). Chinner (1960) first discussed the occurrence of staurolite and kyanite in the sillimanite-muscovite zone of Glen Clova. He suggested, from textural observations, that staurolite and kyanite formed during a retrograde stage of metamorphism. All regional metamorphic pelitic gneisses from this study are of sillimanite-muscovite grade with retrograde development both of kyanite after sillimanite and of zincian staurolite. The post regional metamorphic intrusion of the Glen Doll diorite led to the development of a local contact aureole within a regional metamorphic terrain. This intrusion can be assigned to the 'Newer granites' the age of which is approximately 400 Ma (e.g. Chinner, 1966).

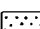

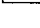
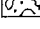
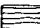

The metamorphosed pelites from within the contact aureole provide the opportunity to examine the phase relations of the breakdown of zincian staurolite which occurred during the contact metamorphic stage. Breakdown reactions of zincian and Zn-free staurolite from other areas have been discussed by various authors (e.g. Guidotti, 1965; Loomis, 1972; Kwak, 1974; Atkin, 1978; Stoddard, 1979; Yardley and Long, 1981). Kwak (1974) criticizes the fact that numerous breakdown reactions of zincian staurolite are given in the literature, but few cited reactions account for Zn in the product phases. In this study one of the product phases is Zn-rich spinel which formed together with magnetite, andalusite, and biotite as the result of an oxidation reaction of the zincian staurolite, muscovite, and quartz. This paper presents information on the regional and contact metamorphic development of the staurolite-bearing gneisses and suggests continuous and discontinuous reactions that led to the termination of the assemblage zincian staurolite + muscovite + quartz.

### *Geological setting*

The metamorphosed pre-Devonian sedimentary and volcanic rocks of the Glen Doll/Glen Clova area (fig. 1) belong to the Dalradian succession. Stratigraphic correlations of the rocks from the Glen Doll/Glen Clova area with well-known Dalradian units from the Blair Atholl/Loch Tummel area (Harris and Pitcher, 1975) are uncertain. However, within the mapped area of 25 km<sup>2</sup> to the south and south-west of the Glen Doll diorite (fig. 1) migmatites are assigned to the Ben Lui Schists (Bradbury, 1979) and the carbonate-rich rocks at Corrie Sharroch (Dürig, 1981) may correlate with the Loch Tay Limestone (middle Dalradian). Inhomogeneous amphibolite horizons are the stratigraphic equivalents of the 'Green Beds' (e.g. van de Kamp, 1970), which belong to the Southern Highland Group (upper Dalradian). Harte and Johnson (1968) showed that the structural history is a result of at least three phases of deformation with various periods of mineral development.

Generalized geological map of the  
Glen Doll-Glen Clova area

**Legend**

-  Diorite
-  Contact aureole
-  Pelitic and psammitic gneisses
-  Inhomogeneous amphibolites
-  Homogeneous amphibolites
-  Quartzporphyries
-  Quaternary cover

0 1 km

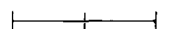
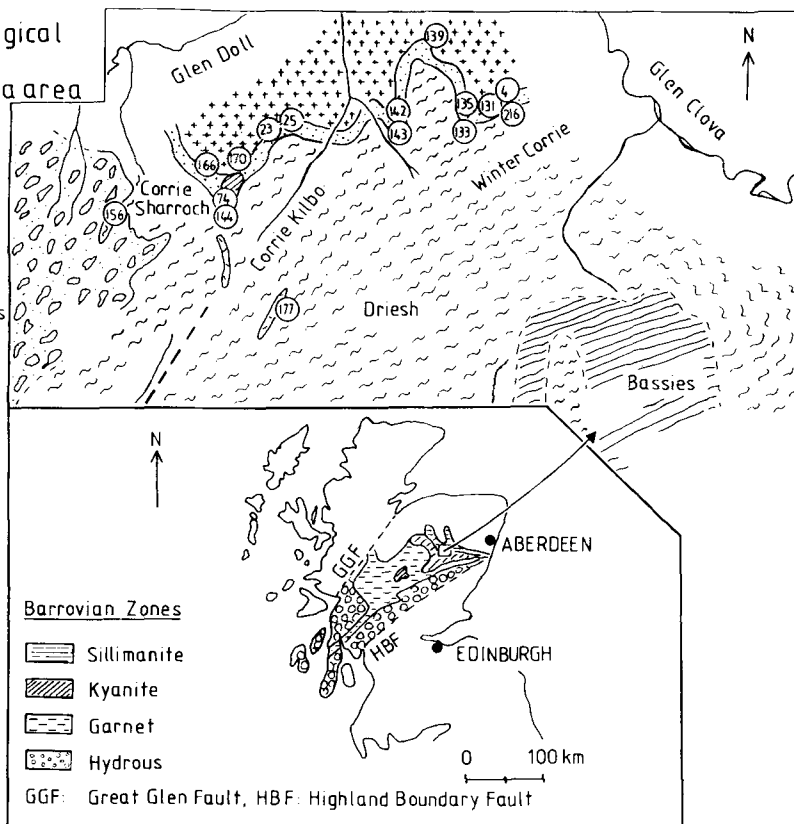



FIG. 1. Generalized geological map of the Glen Doll-Glen Clova area with localities of the samples discussed in the text. Samples 158 and 177 are the regional metamorphic gneisses which were used for geobarometry and geothermometry. Dashed lines indicate uncertain contacts based on outcrops. Inset: Map showing the Barrovian metamorphic zones of the Grampian Caledonides (redrawn after Johnson, 1963) and the location of the study area. The chlorite and biotite zones are combined as hydrous zones.

The study area was first investigated by Barrow (1893, 1912a, b), who recognized the importance of the so-called index minerals such as staurolite and the  $Al_2SiO_5$  polymorphs as indicators of the pressure and temperature of metamorphism (Barrow, 1893). The regional metamorphic rocks in this study are from the north of the sillimanite-muscovite isograd (Chinner, 1965) (fig. 1). This zone represents the highest grade of a metamorphic sequence characterized by reactions along chlorite, biotite, garnet, staurolite, and kyanite (Chinner, 1965) isograds (fig. 1; note that the chlorite and biotite zones are combined as hydrous zones).

According to Bradbury (1979), textural relationships show a coevality of the peak of Barrovian metamorphism and migmatization with an approximate age of  $514 \pm 6/-7$  Ma (U-Pb zircon age). Some 100 Ma after this Grampian metamorphic event, during uplift, the cooled regionally

metamorphosed rocks were intruded by the Glen Doll plutonic complex. This complex is a diorite with minor variations towards gabbroic and granodioritic compositions (Barrow, 1912b). The contact of the Glen Doll intrusion is nearly concordant with the shallow dipping country rock (Chinner, 1962). As a result the contact and the surrounding metamorphic aureole are irregular.

#### Metamorphic history

The metamorphic development of the rock series comprises three major metamorphic stages (I to III, fig. 2); prograde mineral growth included early formation of staurolite and kyanite and was followed by growth of fibrolitic sillimanite. Even though staurolite and kyanite were not stable at this metamorphic stage, small relict grains of staurolite and kyanite are found as inclusions within the cores of garnet porphyroblasts as well as

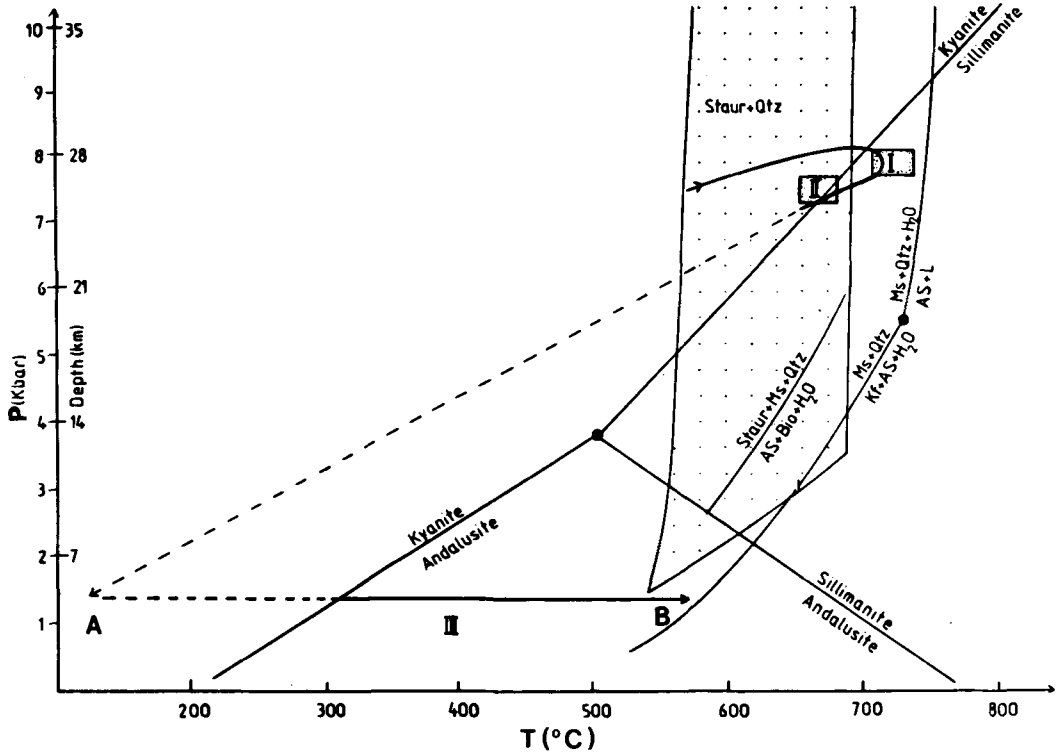


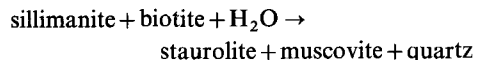
FIG. 2.  $P$ - $T$  diagram showing the schematic metamorphic path of the regional and contact metamorphic gneisses. The  $\text{Al}_2\text{SiO}_5$  triple-point after Holdaway (1971); univariant reaction curve  $\text{Staur} + \text{Ms} + \text{Qtz} \rightarrow \text{As} + \text{Bio} + \text{H}_2\text{O}$  after Hoschek (1969); stability fields of  $\text{Staur} + \text{Qtz}$  after Richardson (1968); of  $\text{Ms} + \text{Qtz} \geq 3$  kbar after Huang and Wyllie (1974) and  $\leq 3$  kbar after Chatterjee and Johannes (1974). Symbols: I, II, and III: metamorphic stages (see text); A: estimated metamorphic conditions of the outermost contact aureole; B: metamorphic conditions of the inner contact aureole.

relics within muscovite (kyanite, staurolite) and plagioclase (kyanite). The staurolite inclusions are too small for microprobe analysis, so that their Zn content is presently unknown. Needles of sillimanite are included in rims of garnet and tourmaline and in cores of plagioclase ( $\text{An}_{30}$ ), quartz, and tourmaline. In addition, fibrolitic sillimanite occurs in the matrix of gneisses with the appropriate bulk composition, which further suggests that this was the last prograde aluminosilicate to form. Garnet is commonly present in the sillimanite-muscovite rocks (Chinner, 1960, 1962). An upper estimate of 7.5–8 kbar and 720–740 °C for the metamorphic stage I is based on the stability fields of muscovite + quartz and sillimanite for  $a_{\text{H}_2\text{O}} = 1$  (fig. 2).

Stage II comprises a second period of staurolite and kyanite growth that followed the peak of Barrovian metamorphism (fig. 2). Staurolite and kyanite from this growth stage are texturally distinct from those of stage I and occur as porphyroblasts within patches of fibrolitic sillimanite. Most

of the staurolite and kyanite porphyroblasts give no clear-cut evidence for the mineral growth sequence. However, a few staurolite porphyroblasts contain oriented sillimanite needles that can be traced to and matched with the fabric of the fibrolitic matrix (fig. 3). Similar textures have been noted by Chinner (1960). This clearly shows that the second period of staurolite and kyanite growth postdates sillimanite formation.

The source of Zn for the staurolites is unknown and most of the common rock-forming silicates can hold only minute amounts (e.g. Kwak, 1974). Perhaps Zn which can be found in small quantities in biotite (Haak, 1969; Haak *et al.*, 1984; Dietvorst, 1980) could be incorporated in retrograde staurolite via the well-known reaction:



(Chinner, 1965; Hoschek, 1969; Hess, 1969; Guidotti, 1970; Kwak, 1974).

The biotites that coexist with the zincian staurolite do not have detectable ZnO contents and textures in the rocks do not preclude the possibility that the above reaction occurred as a cycle of coupled reactions as proposed by Carmichael (1969). Alternatively, if Zn was present in the intergranular fluid phase one might reason that the newly formed retrograde staurolite would incorporate Zn. This is due to the high preference of Zn for the tetrahedral site in staurolite (Albee, 1972).



FIG. 3. Regional metamorphic gneiss (sample 177) showing grains of kyanite (Ky) and staurolite (S) within patches of fibrolitic sillimanite (Sill) and surrounded by muscovite (M), biotite (B), and quartz (Q). Inclusions of sillimanite needles can be seen within the upper part of the staurolite grain and within some quartz mosaics.

Geothermometry based on Fe-Mg exchange between garnet and biotite (Thompson, 1976; Holdaway and Lee, 1977; Ferry and Spear, 1978) gives metamorphic temperatures of 650 to 690 °C if rim analyses of garnets and near-rim analyses of biotites are used (Dürig, 1981). The distribution of Ca between garnet and plagioclase in the assemblage quartz-garnet-plagioclase- $Al_2SiO_5$  is used as a geobarometer (Ghent, 1977 and Newton and Haselton, 1981). Since Newton and Haselton proposed equations to calculate the activities of the  $CaAl_{2/3}SiO_4$  component of garnet (Newton and Haselton, 1981) and of plagioclase (Haselton and Newton, 1980) their model was preferred in respect to Ghent's model in which the activity terms were neglected. Application of Newton and Haselton's geobarometer gives pressures between 6.9 and 7.6 kbar for the assemblage with kyanite. These temperatures and pressures might give evidence that staurolite and kyanite of stage II were in equilibrium

with the matrix minerals (garnet, biotite, plagioclase) from stage I.

Retrograde growth of chlorite and white mica aggregates gives evidence for the continuation of regional uplift and cooling subsequent to stage II. The intrusion of the Glen Doll diorite reheated the regionally metamorphosed rocks within the contact aureole, which, on the basis of the contact metamorphic mineral andalusite, has an estimated width of about 200 m within the study area. Stage III represents the mineral growth which took place in the contact aureole and it is characterized by a high-temperature gradient from the outer aureole (see A in fig. 2) to the inner aureole (see B in fig. 2) in which pyroxene-hornfels conditions were reached.

Chinner (1962) described the breakdown of almandine-rich garnets whereas garnets with slightly increased pyrope content are stable within the contact aureole. In contact metamorphic reactions involving aluminosilicates, kyanite and sillimanite either invert to andalusite or participate in more complex reactions involving garnet, cordierite, K-feldspar, biotite, and spinel (Chinner, 1962, 1978).

Reaction textures show the breakdown of staurolite, garnet, kyanite, and sillimanite and growth of andalusite (in addition to other minerals which will be discussed later) in rocks from the outer aureole. Abundance of muscovite and especially biotite can be ascribed to a strong flux of water from the dehydrating inner aureole, in which muscovite is virtually absent (Chinner, pers. comm.). However, biotite as a hydrous mineral is still an important constituent in the inner aureole. The approach of the metamorphic path towards the upper thermal stability of muscovite + quartz (fig. 2) and the stability of andalusite indicate that a temperature range from about 200 °C in the outermost to 600 °C in the innermost contact aureole and pressures of about 1 to 2.5 kbar were the possible *P-T* conditions of the contact metamorphic stage III.

#### *Breakdown of zincian staurolite in the Glen Doll aureole*

*Petrography and textures.* Samples taken across the aureole show progressive mineralogical and textural changes and give 'snapshots' of the progression of contact metamorphism. Within the outer aureole the regional metamorphic assemblages and textures are preserved to a large extent. Contact metamorphic reactions can be reconstructed with the help of relict minerals, pseudomorphs, and reaction textures. Representatives of gneisses from the outer aureole are samples 133 and 216 from Winter Corrie, samples 142, 143 from the east

slope of Corrie Kilbo, and sample 144 from about 200 m east of Corrie Sharroch (fig. 1). In the field, these rocks could easily be mistaken for regional metamorphic gneisses. However, they typically contain black veins and lenses composed of dense, fine-grained material. In thin-section these veins predominantly consist of minerals of contact metamorphic origin. These are fine-grained, partly pinitized cordierite, corundum, andalusite, green spinel, and abundant magnetite. Some small kyanite relics occur within andalusite which formed through polymorphic inversion. Corroded biotite and kyanite are surrounded by cordierite and spinel. Chinner (1978) described this reaction texture with orthoclase as product phase. Orthoclase was not recognized in the thin-sections discussed here. Some fibrolitic sillimanite is converted to andalusite or replaced by white mica. Porphyroblasts of plagioclase (An<sub>30</sub>) in sample 133 enclose a microfolded internal schistosity composed of quartz, garnet (not found in the matrix), tourmaline, biotite, muscovite, magnetite, kyanite, and apatite. This might indicate stage III growth of plagioclase. The different stages of breakdown of zincian staurolite can be observed in samples 133 and 216 and will be described in more detail in a later section.

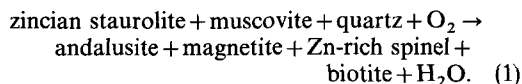
Massive hornfels of the *inner contact aureole* form a narrow band next to the diorite. Due to lack of exposures, the hornfels outcrops are not always conspicuous in the field. Hornfels samples are from the western slope of the Scorrie (samples 4, 131, 135, 139, fig. 1) and from the east of Corrie Sharroch (samples 74, 166, 170). In contrast to the gneisses from the outer aureole, inner aureole samples are richer in cordierite, corundum, and spinel, and K-feldspar appears as additional phase. The abundance of corundum and K-feldspar could be attributed to the breakdown of muscovite following the reaction muscovite → corundum + K-feldspar + H<sub>2</sub>O. The breakdown of zincian staurolite is completed. The further progressed stage of contact metamorphism is characterized by the development of a granular texture and a predominantly anhydrous mineralogy with coarse-grained quartz, andalusite, and magnetite in addition to cordierite, corundum, green spinel, K-feldspar, and plagioclase.

The occurrence of assemblages with either corundum or quartz in different layers within the same thin-section indicates that large scale equilibrium has not been achieved. Thus, application of geothermometry and geobarometry is not adequate. However, the small domains in which the contact metamorphic reactions appear to be completed are likely to have reached equilibrium.

*Continuous and discontinuous reactions.* Textural

evidence for the breakdown of zincian staurolite under contact metamorphic conditions of the outer aureole is as follows: the staurolite grains are always rimmed by andalusite (fig. 4A-D) and small flakes of biotite are present (fig. 4B-C); small grains of Zn-rich spinel and/or magnetite are found in the cracks of the staurolite grains and next to andalusite (fig. 4A-D); muscovite plates generally are in grain contact with andalusite and with Zn-rich spinel but not with staurolite (fig. 4A, C, D).

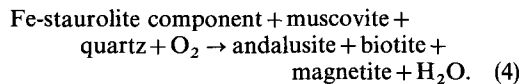
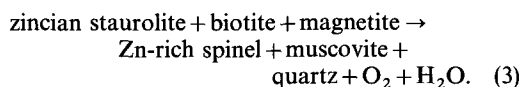
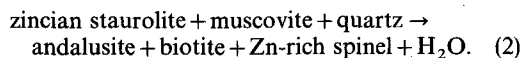
The textures suggest a breakdown reaction which involves all the phases associated with zincian staurolite:



These phases can be satisfactorily described in terms of eight components (K-Zn-Fe-Mg-Al-Si-H-O). Assuming that *P* remained constant, reaction 1 would occur at a specified *T* and would be invariant in this system of components.

The reaction did not go to completion everywhere and some nearly intact staurolite grains with only small rims of andalusite, Zn-rich spinel, magnetite, and biotite are present (fig. 4A). The majority of staurolite grains, however, form small relics (fig. 4B) and a few are almost completely consumed (fig. 4C). As shown in fig. 4B and C 'shimmer aggregates' (white mica) are also present, presumably as a result of late retrograde hydration of relict staurolite. Microprobe analyses of staurolites and their breakdown products, Zn-rich spinel (with up to 14 wt. % ZnO), magnetite, andalusite, and biotite, are given in Table II.

Textures indicate the possibility of three continuous reactions which are among the potential continuous reactions leading to reaction 1:



Microprobe data and textural criteria which are discussed in more detail below suggest that oxidation is one of the driving forces of the breakdown of the staurolites from the Glen Doll aureole. Thus, reaction 3, where magnetite is consumed and where oxygen is on the product side of the reaction, is not relevant in this study. Slight variations in Zn-Fe-Mg contents of the individual staurolite grains as well as the availability of oxygen might determine

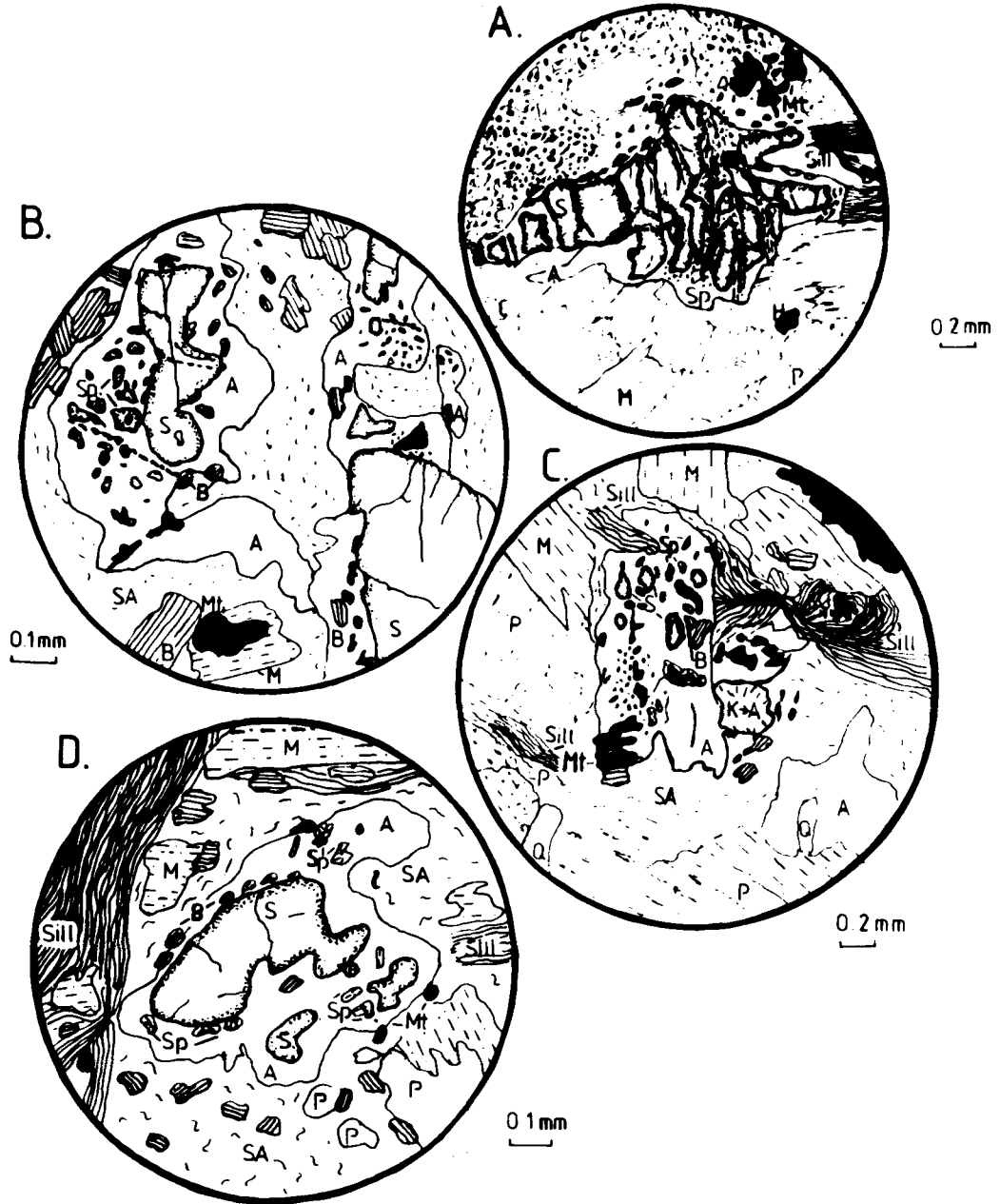


FIG. 4. Thin-section drawings showing the different stages of staurolite breakdown. A: Nearly intact staurolite (S) with reaction rim of andalusite (A), magnetite (Mt, some oxidized to haematite, H), minor amounts of Zn-rich spinel (Sp), and biotite flakes (B, not shown within the reaction rim due to small grain size). In the upper left corner Mt, chlorite (dot-dash pattern), and plagioclase (patternless matrix) may pseudomorph oxidized garnet. B: Advanced stage of staurolite breakdown showing the formation of andalusite (A), biotite (B), and magnetite (Mt) followed by Zn-rich spinel (Sp) which encloses some Mt grains. Sillimanite (Sill) and 'shimmer aggregate' (SA) are also shown. C: Staurolite (S) is almost completely replaced by andalusite (A) and nearly equal amounts of magnetite (Mt) and Zn-rich spinel (Sp). As in B some Mt is surrounded by Sp. Sillimanite (Sill), 'shimmer aggregate' (SA), plagioclase (P), quartz (Q), and kyanite (K) converting to andalusite (A) are found in the matrix. D: Corroded staurolite (S) rimmed by andalusite (A), biotite (B), and Zn-rich spinel (Sp). Only three magnetite grains (Mt) occur at the edge of the reaction rim (see text for explanation). Sillimanite (Sill), plagioclase (P), muscovite (M), and 'shimmer aggregate' (SA) are found in the matrix.

ZINCIAN STAUROLITE

Table I. Representative microprobe analyses of regional metamorphic minerals

Sample No.	Garnet			Biotite			Muscovite		Plagioclase			Staurolite			
	158 1R WDS	158 1C WDS	177-1 3R WDS	177-1 3C/R WDS	177-1 II/3b EDS	158 4 WDS	158 3/C WDS	177-1 1b,R EDS	158 5R WDS	158 5C WDS	177-1 5C/R WDS	177-1 5C/R WDS	177-1 5C/R WDS		
SiO <sub>2</sub>	37.30	37.61	37.32	37.60	37.44	35.40	35.28	46.63	61.50	59.43	SiO <sub>2</sub>	27.65	27.44	27.48	27.81
TiO <sub>2</sub>	0.02	-	-	0.01	-	1.96	1.94	0.48	-	-	TiO <sub>2</sub>	0.33	0.53	0.27	0.19
Al <sub>2</sub> O <sub>3</sub>	20.90	21.02	21.07	21.03	20.50	17.50	18.46	35.37	23.26	24.63	Al <sub>2</sub> O <sub>3</sub>	54.74	55.14	52.64	53.76
Cr <sub>2</sub> O <sub>3</sub>	0.03	0.03	0.03	0.02	-	0.02	-	-	-	-	Cr <sub>2</sub> O <sub>3</sub>	0.05	0.05	-	0.02
FeO	34.27	34.36	34.37	34.25	33.55	20.01	20.07	0.86	0.31	-	FeO	12.03	12.19	14.00	11.50
MnO	1.75	1.78	1.88	1.92	2.11	-	-	0.03	-	-	MnO	0.12	0.09	0.03	0.06
MgO	2.81	3.15	3.23	3.10	3.26	9.75	10.42	0.54	-	-	MgO	1.29	1.19	1.92	1.64
CaO	2.88	2.63	2.73	2.24	2.36	-	-	0.03	6.30	6.38	CaO	0.01	0.01	-	-
Na <sub>2</sub> O	-	-	-	-	-	-	-	0.82	8.36	8.50	ZnO	1.44	1.54	0.60	1.18
K <sub>2</sub> O	-	-	-	-	-	9.25	9.61	9.21	0.09	0.15	K <sub>2</sub> O	0.03	0.01	0.14	0.01
	99.96	100.58	100.63	100.17	99.25	93.89	95.78	93.97	99.92	99.09	Total	97.69	98.19	97.08	96.17
	Cations per 12 oxygens			Cations per 11 oxygens			Cations per 8 oxygens			Cations per 23 oxygens					
Si	3.002	3.004	2.978	3.014	3.028	2.744	2.684	3.114	2.742	2.677	Si	3.824	3.778	3.866	3.901
Al IV	-	-	0.022	-	-	1.256	1.316	0.887	1.228	1.308	Al IV	0.176	0.222	0.134	0.099
Al VI	1.983	1.979	1.960	1.987	1.954	0.343	0.340	1.898	-	-	Al VI	8.751	8.727	8.596	8.790
Ti	0.001	-	-	-	0.001	0.114	0.111	0.024	-	-	Ti	0.033	0.055	0.029	0.020
Fe 3+	0.008	0.012	0.060	-	-	-	-	-	-	-	Cr	0.005	0.005	-	0.002
Cr	0.002	0.002	0.002	0.002	0.001	0.002	-	-	-	-	Mg	0.266	0.265	0.402	0.343
Mg	0.337	0.375	0.384	0.370	0.393	1.126	1.182	0.052	-	-	Fe	1.391	1.404	1.648	1.350
Fe 2+	2.299	2.283	2.233	2.296	2.269	1.297	1.277	0.048	-	-	Mn	0.014	0.011	0.003	0.007
Mn	0.119	0.120	0.127	0.130	0.145	0.004	-	-	-	-	Zn	0.150	0.156	0.063	0.122
Ca	0.248	0.225	0.233	0.192	0.204	-	-	0.002	0.301	0.308	Sum	14.610	14.623	14.741	14.634
Na	-	-	-	-	-	-	-	0.106	0.723	0.743					
K	-	-	-	-	-	0.915	0.933	0.785	0.005	0.009					
Sum	7.999	8.000	7.999	7.991	7.995	7.801	7.843	6.915	4.999	5.045					

+ = Total iron as FeO  
 R = Rim analysis  
 C = Core analysis  
 WDS = Wavelength dispersive spectrometer  
 EDS = Energy dispersive spectrometer

Table II. Representative microprobe analyses of minerals from within the contact aureole

Sample No.	Biotite			Muscovite			Sillimanite	Plagioclase		
	133	133	133	133	133	133	133	133	133	133
Analyses No.	I/1,R/C	I/1,C	I/1,R	2/R	2/C	I/1R	2	2	I/1a	I/1b
Spectrometer	EDS	EDS	EDS	WDS	WDS	EDS	WDS	WDS	EDS	EDS
SiO <sub>2</sub>	35.10	35.02	33.82	47.11	46.81	45.33	37.09	63.14	61.24	61.02
TiO <sub>2</sub>	3.25	3.27	3.22	0.63	0.94	1.49	0.02	-	0.13	-
Al <sub>2</sub> O <sub>3</sub>	19.12	18.97	19.66	34.04	33.76	33.31	62.79	23.87	23.51	23.48
Cr <sub>2</sub> O <sub>3</sub>	-	-	-	0.03	0.03	-	0.02	0.03	-	-
FeO <sup>+) )</sup>	19.73	19.95	20.44	1.71	1.76	1.98	0.21	0.06	-	-
MnO	-	-	0.34	-	-	-	-	-	-	-
MgO	9.88	9.19	9.23	0.58	0.63	2.92	0.05	-	-	-
CaO	-	-	-	0.42	-	-	-	5.52	5.47	5.56
Na <sub>2</sub> O	-	-	-	0.42	0.69	-	-	7.02	8.67	8.55
K <sub>2</sub> O	9.78	9.75	9.71	10.03	9.97	10.41	-	0.48	0.52	0.42
Total	96.87	96.15	96.42	94.55	94.59	95.44	100.18	100.12	99.54	99.03
Si	2.638	2.655	2.573	3.151	3.136	3.032	1.999	2.782	2.740	2.741
Al <sup>IV</sup>	1.362	1.345	1.427	0.849	0.864	0.968	0.001	1.239	1.239	1.243
Al <sup>VI</sup>	0.332	0.350	0.336	1.835	1.802	1.658	3.989	-	-	-
Ti	0.184	-	0.184	0.032	0.048	0.075	-	-	-	-
Cr	-	-	-	0.002	0.002	-	0.001	-	-	-
Mg	1.107	1.039	1.047	0.058	0.063	0.292	-	-	-	-
Fe	1.234	1.265	1.301	0.096	0.099	0.111	0.010	-	-	-
Mn	-	-	0.022	-	-	-	-	-	-	-
Ca	-	-	-	-	-	-	-	0.261	0.262	0.268
Na	-	-	-	0.055	0.090	-	-	0.600	0.752	0.745
K	0.938	0.943	0.942	0.856	0.852	0.888	-	0.027	0.030	0.024
Sum	7.795	7.597	7.832	6.934	6.956	7.024	6.000	4.909	5.023	5.021

Sample No.	Zinc-rich spinel			Staurolite								
	133	133	133	133	133	133	133	133	133	133	216	216
Analyses No.	2	II-1	II-2	N17R	N18R/C	N19C	N20C	N21R/C	N22R	I/1R	N16C	N18R
Spectrometer	WDS	EDS	EDS	WDS	WDS	WDS	WDS	WDS	WDS	EDS	WDS	WDS
SiO <sub>2</sub>	-	-	-	28.17	28.08	27.99	27.92	27.93	28.02	27.61	28.10	27.72
TiO <sub>2</sub>	0.14	-	-	0.18	0.23	0.30	0.31	0.28	0.37	0.67	0.45	0.51
Al <sub>2</sub> O <sub>3</sub>	57.12	59.32	57.73	54.76	54.14	54.07	54.33	54.23	54.66	54.94	54.94	53.98
Cr <sub>2</sub> O <sub>3</sub>	-	0.35	4.13	-	0.03	0.07	-	0.04	0.05	0.22	0.01	0.02
FeO <sup>+) )</sup>	26.85	27.49	24.07	9.43	10.97	10.65	10.62	10.74	10.52	10.00	11.21	11.36
MnO	0.04	0.59	0.61	0.24	0.36	0.01	0.34	0.37	0.34	-	1.10	1.13
NiO	-	-	-	0.03	0.06	0.03	-	-	-	-	0.03	-
MgO	4.44	3.65	4.13	1.15	1.75	1.73	1.68	1.81	1.82	1.40	2.13	2.28
CaO	0.03	-	-	-	0.01	-	-	0.01	0.01	-	0.01	-
ZnO	11.47	9.89	14.28	1.97	1.27	1.57	1.57	1.65	1.70	2.41	0.81	0.83
Total	100.09	101.28	101.15	95.92	96.90	96.42	96.77	97.08	97.49	97.25	96.71	97.83
	<u>3 cations</u>			<u>Cations per 23 oxygens</u>								
Si	-	-	-	3.934	3.907	3.907	3.887	3.883	3.874	3.829	3.928	3.837
Al <sup>IV</sup>	-	-	-	0.066	0.093	0.093	0.113	0.117	0.126	0.171	0.072	0.163
Al <sup>VI</sup>	1.924	1.971	1.932	8.948	8.776	8.803	8.803	8.769	8.781	8.809	8.637	8.643
Ti	0.003	-	-	0.019	0.024	0.031	0.032	0.029	0.038	0.070	0.047	0.053
Fe <sup>3+</sup>	0.073	0.021	0.060	-	-	-	-	-	-	-	-	-
Cr	-	0.008	0.008	-	0.003	0.008	-	0.004	0.005	0.024	0.001	0.002
Mg	0.189	0.153	0.175	0.239	0.363	0.360	0.349	0.375	0.375	0.289	0.444	0.470
Ni	-	-	-	0.003	0.007	0.004	-	-	-	-	0.004	-
Fe	0.568	0.627	0.511	1.101	1.277	1.243	1.237	1.249	1.216	1.160	1.311	1.315
Mn	0.001	0.014	0.015	0.028	0.042	0.001	0.040	0.044	0.040	-	0.130	0.133
Zn	0.242	0.206	0.299	0.203	0.130	0.162	0.161	0.169	0.174	0.247	0.084	0.085
Ca	-	-	-	-	0.001	-	-	0.001	0.001	-	0.002	-
Sum	3.000	3.000	3.000	14.541	14.623	14.612	14.622	14.640	14.630	14.599	14.660	14.701

Symbols as in table I



which of the continuous reactions, 2 or 4, would first be operative as the physical conditions approached those of reaction 1.

The reactions described above may provide an explanation of zoning in the staurolite. Microprobe analyses of a staurolite porphyroblast, which has andalusite, magnetite, biotite, and minor Zn-rich spinel as breakdown products, show a slight but consistent increase in zinc content at the rim (Table II and fig. 5). The amount of Zn in the individual staurolite grains varies from 0.70 to 2.40 wt. % ZnO. In contrast to this staurolites from regional metamorphic gneisses about 800 m away from the contact aureole are essentially unzoned although different grains might have variable Zn contents (Table I) and, thus, the zoning is attributed to the contact metamorphism. Reaction 4 provides a possible mechanism to explain the enrichment of Zn at the rims of some staurolite grains from the contact aureole (fig. 5). If the breakdown of staurolite started with continuous reaction 4 in which Zn-rich spinel is not present, then the Zn-staurolite component would begin to concentrate in the unreacted staurolite (fig. 6A-C). Apparently, the rock did not remain at high temperatures long enough to allow the Zn to distribute homogeneously through the staurolite grain, and zoning was preserved. The possibility that some of the Zn-rich spinel formed later than the magnetite is supported by the presence of magnetite grains rimmed by Zn-rich spinel (fig. 4B and c) in some parts of samples 133 and 216.

In the breakdown products of a few staurolite grains the ratio of the Zn-rich spinel to magnetite is much higher than commonly is the case. This feature can be explained if the staurolite first began to break down via continuous reaction 2 to form Zn-rich spinel (fig. 6). Magnetite formation would have begun after the physical conditions exceeded

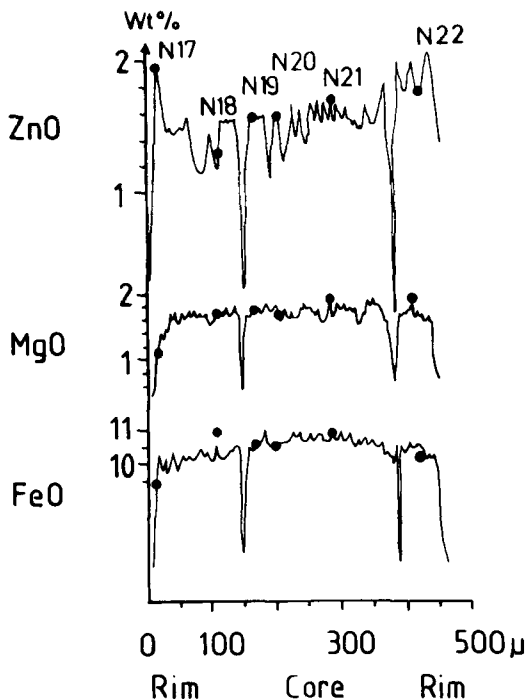


FIG. 5. Line scan through a staurolite porphyroblast from a contact metamorphosed gneiss (sample 133) showing an increase in ZnO and a decrease in MgO and FeO content at the rims. Analyses of microprobe points N17 through N22 are given in Table II.

staurolite + muscovite + quartz +  $O_2$  stability and the staurolite still remaining in the rock began to break down via discontinuous reaction 1. It would be expected that the staurolites which are predominantly surrounded by Zn-rich spinel would show a decrease in Zn content towards the rim. As

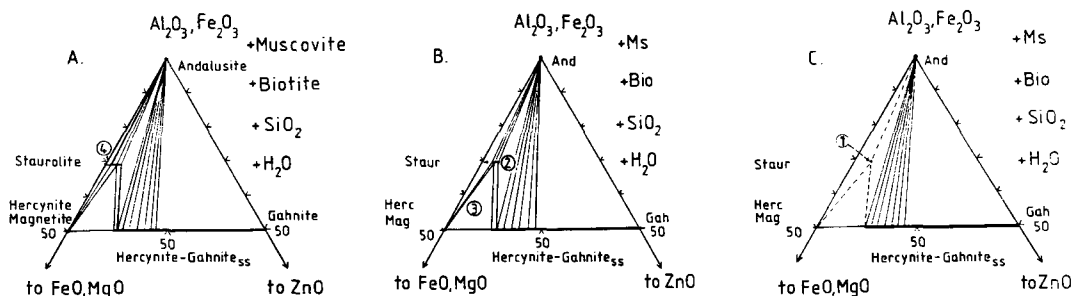


FIG. 6. Part of the system K-Zn-Fe-Mg-Al-Si-H-O projected from muscovite, biotite,  $SiO_2$ , and  $H_2O$  to part of an  $(Al_2O_3 + FeO)-(FeO + MgO)-ZnO$  ternary. The projection shows the effect of the Zn content on the staurolite breakdown reaction and possible phase relations. A: shows the initial stage of continuous reaction 4; B: shows continuous reaction 2 and 3 leading to discontinuous reaction 1; C: shows discontinuous reaction 1. See text for detailed discussion.

an example a staurolite porphyroblast from sample 216 was analysed (Table II); however, the Zn content was so low that no clear evidence for this concept could be obtained.

Mineral analyses of the regional metamorphic equivalents to the rocks discussed here (Table I) support the observation that oxygen is added to the system during contact metamorphism. None of the regional metamorphic rock-forming minerals contain sufficient  $\text{Fe}^{3+}$  to form the large amounts of magnetite that are found in the contact metamorphic rocks. Stable almandine-rich garnet is reported from other parts of the contact aureole (Chinner, 1962). In all samples from this part of the contact aureole, regional metamorphic garnet [ $\text{Alm}_{75}\text{Pyr}_{13}(\text{Gross} + \text{Andr})_7\text{Spess}_5$ ], which is common in the country rock, is not found in the matrix. Pseudomorphs which predominantly consist of magnetite, chlorite, muscovite, and plagioclase (Table II) could represent the oxidized breakdown products of garnets.

As shown by Chinner (1962) the oxidizing or reducing potential of the fluid during the contact metamorphic stage depends on the original oxygen content of the rock. In regional, haematite-bearing gneisses (Chinner, 1960) contact metamorphism in the outer Glen Doll aureole led to the reduction of haematite to magnetite. However, the rocks discussed here apparently contained mostly ferrous iron some of which was oxidized to form magnetite as can be clearly seen from reaction textures. This supports Chinner's observations that the  $f_{\text{O}_2}$  of the intergranular fluid was less than that of the haematite/magnetite buffer.

At the pressures of 1 to 2.5 kbar suggested above for the Glen Doll contact aureole and at oxygen fugacities below that of the NNO buffer, cordierite should have formed as a breakdown product of staurolite (Ganguly, 1972). As mentioned earlier cordierite is a typical contact metamorphic mineral in the hornfels from the Glen Doll aureole; however, in only one sample (216) was cordierite found within the small domain of staurolite breakdown. This suggests  $f_{\text{O}_2}$  was higher than the NNO buffer. Chinner (pers. comm.) has observed rims of spinel and cordierite around staurolite grains in rocks from other localities of the Glen Doll aureole and he suggests that staurolite and biotite formed Zn-rich spinel, cordierite, and  $\text{K}^+$ . This observation raises the possibility of other staurolite breakdown reactions involving cordierite.

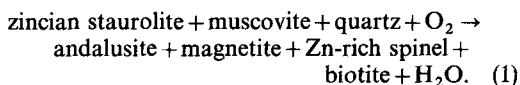
### Conclusions

The metamorphic stages leading to the formation of zincian staurolite from the Glen Doll-Glen Clova area are as follows:

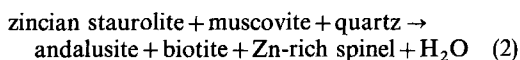
(1) Zincian staurolite together with kyanite formed within fibrolitic sillimanite at a late stage of Barrovian metamorphism. The source of Zn is uncertain.

(2) Regional metamorphism (about 500 Ma) was followed by the intrusion of the Glen Doll diorite complex (about 400 Ma). Contact metamorphism is characterized by a large temperature gradient from the hydrous outer aureole to the dehydrated inner aureole, where pyroxene-hornfels conditions were reached.

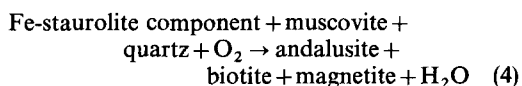
(3) Within the outer contact aureole, zincian staurolite (0.70 to 2.40 wt. % ZnO) broke down by the discontinuous oxidation reaction:



(4) Microprobe data, as well as textural criteria, support the interpretation that slight variations in the Zn-Fe-Mg contents, as well as the availability of oxygen, determined which of the two continuous reactions



or



would first become effective as the physical conditions approached those of the terminal breakdown reaction.

(5) The majority of the staurolites started to break down by continuous reaction 4. This led to the relative increase in zinc in the remaining staurolite that then enabled the formation of Zn-rich spinel with up to 14 wt. % ZnO according to reaction 2.

*Acknowledgements.* I wish to thank J. C. Schumacher for vivid discussions on the work reported above, B. Harte for his support during field work, and M. Raith for his advice during the petrographical work. I also would like to thank G. A. Chinner, M. Raith, J. C. Schumacher, and F. A. Seifert for critically reading the manuscript and D. Ackermann (Mineralogisch-Petrographisches Institut, Kiel) and R. Wohlleben (Forschungsinstitut der Feuerfestindustrie, Bonn) for assistance with the microprobe work.

### REFERENCES

- Albee, A. L. (1972) *Bull. Geol. Soc. Am.* **83**, 3249-68.  
 Atkin, B. P. (1978) *Mineral. Mag.* **42**, 237-9.  
 Barrow, G. (1893) *Q. J. Geol. Soc. Lond.* **49**, 330-58.  
 ——— (1912a) *Proc. Geol. Ass.* **23**, 268-73.  
 ——— (1912b) *Mem. Geol. Surv. Scotl.* 1-138.

- Bradbury, H. J. (1979) In *The Caledonides of the British Isles—reviewed* (Harris, Holland, and Leake, eds.), 351–6.
- Carmichael, D. M. (1969) *Contrib. Mineral. Petrol.* **20**, 244–67.
- Chatterjee, N. D., and Johannes, W. (1974) *Ibid.* **48**, 89–114.
- Chinner, G. A. (1960) *J. Petrol.* **1**, 178–217.
- (1962) *Ibid.* **3**, 316–40.
- (1965) *Mineral. Mag.* **34**, 316–40.
- (1966) *Q. J. Geol. Soc. Lond.* **122**, 159–86.
- (1978) In *Petrology for students* (S. R. Nockolds, R. W. O. B. Knox, and G. A. Chinner, eds.) 343–427.
- Dietvorst, E. J. L. (1980) *Contrib. Mineral. Petrol.* **75**, 327–37.
- Dürig, R. (1981) *Geologie und Petrographie der regional- und kontaktmetamorphen Gesteinsserien in Glen Clova, Kaledoniden, Schottland*. Unpubl. Diplom. thesis, Univers. Kiel.
- Ferry, J. M., and Spear, F. S. (1978) *Contrib. Mineral. Petrol.* **66**, 113–17.
- Ganguly, J. (1972) *J. Petrol.* **13**, 335–65.
- Ghent, E. D. (1977) In *Short Course applications of thermodynamics to petrology and ore deposits* (H. J. Greenwood, ed.) Mineral. Ass. Can. 99–108.
- Guidotti, C. V. (1965) *Geol. Soc. Am. Abstracts*, Fresno Mtg. 27, 1786.
- (1970) *J. Petrol.* **11**, 277–336.
- Haak, U. K. (1969) *Contrib. Mineral. Petrol.* **22**, 83–126.
- Heinrichs, M., Boneß, M., and Schneider, A. (1984) *Ibid.* **85**, 116–32.
- Harris, A. L., and Pitcher, W. S. (1975) In *A correlation of the Precambrian rocks in the British Isles* (A. L. Harris, ed.) Geol. Soc. Lond. Spec. Rept. 6, 52–75.
- Harte, B., and Johnson, M. R. W. (1968) *Scott. J. Geol.* **5**, 54–80.
- Haselton, H. T., and Newton, R. C. (1980) *J. Geophys. Res.* **85**, 6973–82.
- Hess, P. C. (1969) *Contrib. Mineral. Petrol.* **24**, 191–207.
- Holdaway, M. J. (1971) *Am. J. Sci.* **271**, 97–131.
- and Lee, S. M. (1977) *Contrib. Mineral. Petrol.* **63**, 175–98.
- Hoschek, G. (1969) *Ibid.* **22**, 208–32.
- Huang, W. L., and Wyllie, P. J. (1974) *Am. J. Sci.* **274**, 378–95.
- Johnson, M. R. W. (1963) *Geol. en. Mijn.* **42**, 121–42.
- Kwak, T. A. W. (1974) *Contrib. Mineral. Petrol.* **22**, 208–32.
- Loomis, T. P. (1972) *Geol. Soc. Am. Bull.* **83**, 2449–74.
- Newton, R. C., and Haselton, H. T. (1981) In *Thermodynamics of minerals and melts* (R. C. Newton, A. Navrotsky, and B. J. Wood, eds.) 304 pp.
- Richardson, S. W. (1968) *J. Petrol.* **9**, 468–88.
- Stoddard, E. F. (1979) *Am. Mineral.* **64**, 736–41.
- Thompson, A. L. (1976) *Am. J. Sci.* **276**, 425–54.
- van de Kamp, J. A. (1970) *J. Geol.* **78**, 281–303.
- Yardley, B. W. D., and Long, C. B. (1981) *Mineral. Mag.* **44**, 125–31.

[Manuscript received 2 July 1984;  
revised 7 December 1984]